Two-photon absorption of dipolar and quadrupolar oligothiophene-cored chromophore derivatives containing terminal dimesitylboryl moieties: a theoretical (DFT) structure-property investigation

Anissa Amar, Aziz Elkechai, Jean-François Halet, Frédéric Paul, Abdou Boucekkine

Two-photon absorption of dipolar and quadrupolar oligothiophene-cored chromophores derivatives containing terminal dimesitylboryl moieties: A theoretical (DFT) structure-property investigation

Anissa Amar[1], Aziz Elkechai[1], Jean-François Halet[2]*, Frédéric Paul[3]*, Abdou Boucekkine[3]*

[1] *Laboratoire de Physique et Chimie Quantiques, Faculté des Sciences, Université Mouloud Mammeri de Tizi-Ouzou, 15000 Tizi-Ouzou, Algeria*
[2] *CNRS–Saint-Gobain–NIMS, IRL 3629, Laboratory for Innovative Key Materials and Structures (LINK), National Institute for Materials Science (NIMS), Tsukuba, 305-0044, Japan*
[3] *Univ Rennes, CNRS, ISCR UMR 6226, 35042 Rennes, France*

Dedicated to a long-time friend, collaborator, and leading expert on conjugated materials and their optical properties, Prof. Todd B. Marder, on the occasion of his 66th birthday.

A series of dipolar and quadrupolar dimesitylboryl ($BMes_2$) derivatives containing different thiophene oligomers as the central conjugated bridge to which are appended $BMes_2$ substituents at both ends have been investigated theoretically via density functional theory (DFT) and time-dependent (TD) DFT calculations. Results indicate that for all quadrupolar compounds studied the excited state reached by the two-photon absorption (2PA) is the S_2 state which is one-photon forbidden and which corresponds to the HOMO to LUMO+1 electronic transition. When the terminal alkene (double) bonds in the **nV** species, containing *n* thiophene rings in the conjugated bridge, are replaced by alkyne (triple) bonds, giving the **nT** compounds, an increase of the 2PA cross-sections is always stated. Modification of the conjugated linker and addition of trimethylamonium (NMe_3^+) substituents to the phenyl rings of the terminal $BMes_2$ moieties show two 2PA peaks at different wavelengths with the low energy one corresponding to the population of the S2 excited state and the second one to the population of a higher excited state. Substitution of the NMe_3^+ groups by neutral electron-attracting cyano (CN) groups shows lower 2PA cross-sections.

* Corresponding authors: E-mail: jean-francois.halet@univ-rennes1.fr (J.-F.H.), frederic.paul@univ-rennes1.fr (F.P.) and abdou.boucekkine@univ-rennes1.fr (A.B.)

Introduction

During the last decades, numerous dimesitylboryl ($BMes_2$) derivatives have been synthesized and studied for their remarkable photophysical properties by Todd B. Marder and coworkers,[1-6] especially for the non-linear optical (NLO) responses often observed for multipolar derivatives of this kind. Interestingly, high two-photon absorption (2PA) cross-sections have been reported for several series of quadrupolar derivatives. Among the latter chromophores those constituted by a thiophene oligomer acting as a conjugated bridge spanning two terminal dimesitylboryl terminal groups turned out to be quite promising nonlinear absorbers for various applications for which high two-photon absorption (2PA) cross-sections are usually needed, such as photodynamic therapy, data-storage and optical limitation.[7-10] The NLO properties of the latter compounds are mainly due to the $BMes_2$ moiety that acts as a strong π-electron acceptor thanks to the vacant boron p_z orbital, the latter being sterically protected by the bulky mesityl groups tethered to the boron atom, insuring its chemical stability. Given that these derivatives were also fluorescent, exhibiting usually fluorescence quantum yield above 20%,[4] applications in fluorescence bio-imaging were also envisionable after proper functionalization to solubilize these derivatives in water. Accordingly, Todd B. Marder and coworkers recently investigated a series of new water-soluble dimesitylboryl analogues of these compounds bearing four NMe_3^+ groups attached to the terminal $BMes_2$ moieties.[5,6] Interestingly, these charged compounds exhibit very high 2PA cross-sections, much higher than the ones obtained for the analogous neutral systems previously studied as well as stronger fluorescence quantum yields in organic solvents. Remarkably, these derivatives are also fluorescent in water and a good photochemical stability in the water solvent was stated for some of them, allowing their use for bio-imaging purposes. The best bi-photonic absorbers among this series, namely **2TM-NMe$_3^+$** and **5M-NMe$_3^+$** (Scheme 1), are the subject of this study.[1]

[1] Note that the notation used for these compounds in Marder's original papers is kept here.

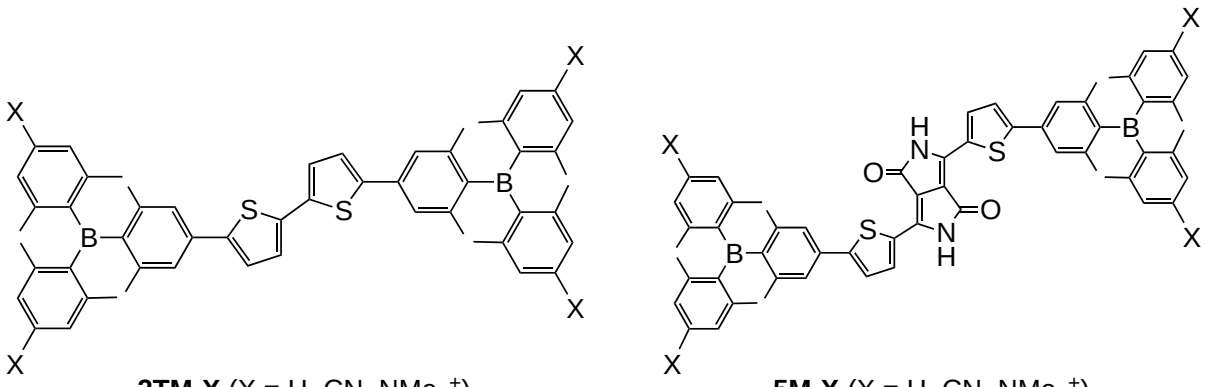

2TM-X (X = H, CN, NMe_3^+) **5M-X** (X = H, CN, NMe_3^+)

Scheme 1 **2TM-X** and **5M-X** series of compounds (X = H, NH_2, CN, NMe_3^+).[5,6]

We have theoretically investigated their 2PA properties trying to understand and rationalize the structural origin of their large NLO responses. Here, we report and discuss results obtained via density functional theory (DFT) and time-dependent (TD) DFT computations on these cationic species and on analogous neutral dimesitylboryl-based quadrupolar systems for comparison, replacing the four NMe_3^+ terminal groups in **2TM-NMe$_3^+$** and **5M-NMe$_3^+$** by hydrogen atoms (**2TM-H** and **5M-H)**, cyanide groups (**2TM-CN** and **5M-CN**) as well as amino groups (**2TM-NH$_2$**). To calibrate our calculations, we start our study considering vinyl (**nV**, *n* = 2-5) and alkyne (**nT**, n = 2-5) related systems previously studied and their dipolar derivatives **2VD**, **4VD**, **2TD** and **4TD** (Scheme 2).[4] These investigations were performed at the DFT level, the computation of the 2PA spectra being carried out using the damped cubic response theory of Jensen and coworkers[11] implemented in the ADF program package.[12] The SAOP Model Potential[13] was used for the 2PA calculations with a DZP basis set, considering the various molecules in the gas phase. Standard PBE0/6-31G(d) computations[14] were also carried out using the Gaussian16 program,[15] in particular for the geometry optimizations in solution (acetonitrile) that cannot be performed with the SAOP model (see ESI).

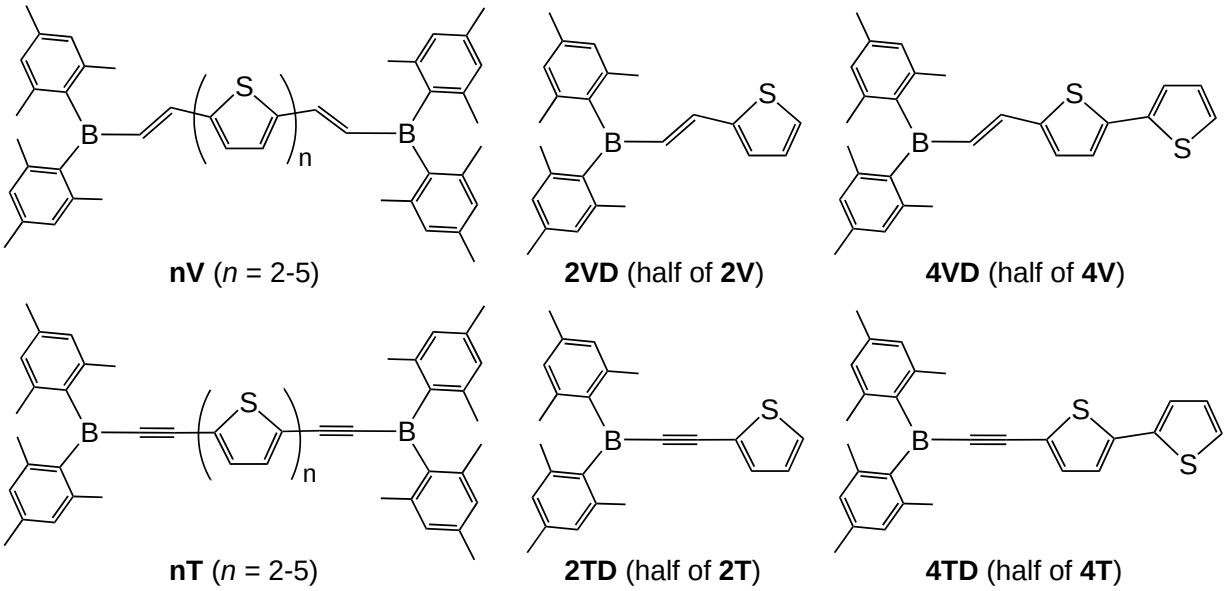

nV (*n* = 2-5) **2VD** (half of **2V**) **4VD** (half of **4V**)

nT (*n* = 2-5) **2TD** (half of **2T**) **4TD** (half of **4T**)

Scheme 2 **nV** and **nT** series of compounds.

Results and Discussion

In order to check the reliability of the computational method that we employed, the one-photon absorption (OPA) and 2PA properties of derivatives **nV** (*n* = 2-5), for which experimental and theoretical data were reported[4] were computed as well as those of the corresponding dipolar sub-systems **2VD** and **4VD** (Scheme 2). For comparison, 2PA properties of the analogous series **nT** (*n* = 2-5) and the corresponding dipolar sub-systems **2TD** and **4TD** (Scheme 2) were also computed to evaluate the effect of triple bonds replacing double bonds in these chromophores. The main results as well as the available experimental data are reported in Table 1, and the simulated 2PA spectra shown in Figure 1. For these quadrupolar systems the excited S2 state is generally one-photon forbidden (or at least approximately forbidden in the case of slight symmetry distortions) and two-photon allowed, as expected for quadrupolar chromophores (Scheme 3).[10,16] The 2PA energy corresponds therefore to the half of the OPA excitation energy to the S2 state. This 2PA-allowed excitation corresponds generally to a HOMO → LUMO+1 transition.

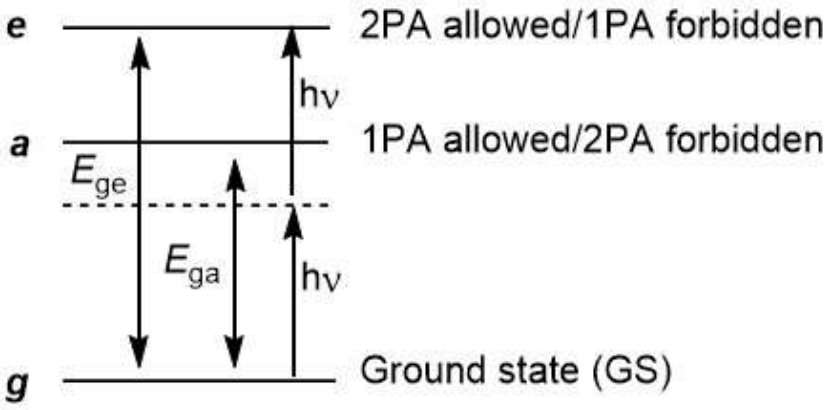

Scheme 3 The three first states of quadrupolar chromophores and transition energies.

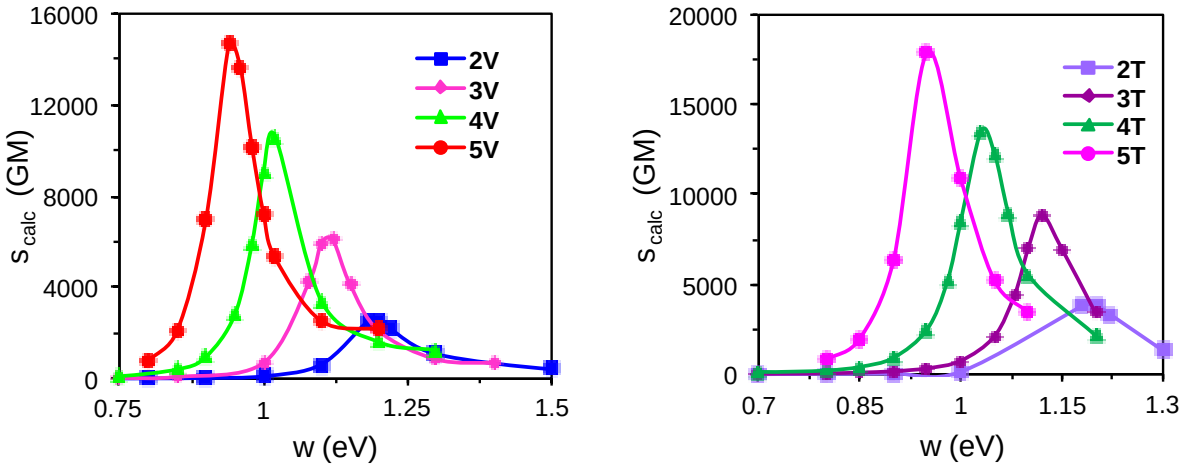

Fig. 1 Simulated 2PA spectra (2PA cross-sections *vs*. frequencies) of the **nV** (*n* = 2-5) and **nT** (*n* = 2-5) series of compounds.

Comparing the computed OPA energies to the experimental values (Table 1), it appears clearly that the SAOP model largely underestimates the HOMO-LUMO gaps. This is not surprising since the SAOP model potential is not based on a hybrid functional but rather on the generalized gradient approximation (GGA) corrected for its asymptotic behavior. Thus, when these gaps are compared to gaps computed at the PBE0/6-31G(d) levels using the same PBE0 optimized geometry, they also appear smaller (Table S1, ESI). This drawback of the SAOP calculations generates in turn a dramatic overestimation of the 2PA cross-sections. We have already quoted this in previous 2PA calculations using the SAOP method with octupolar derivatives.[17] However, it is worth observing that in spite of this overestimated prediction, a very good linear regression coefficient (R^2 = 0.998) is found for the correlation between the

SAOP-computed and experimental values found for the 2PA cross-sections measured in solution (Figure 2). This result gives in turn confidence regarding the reliability of the 2PA trends given by the SAOP model.

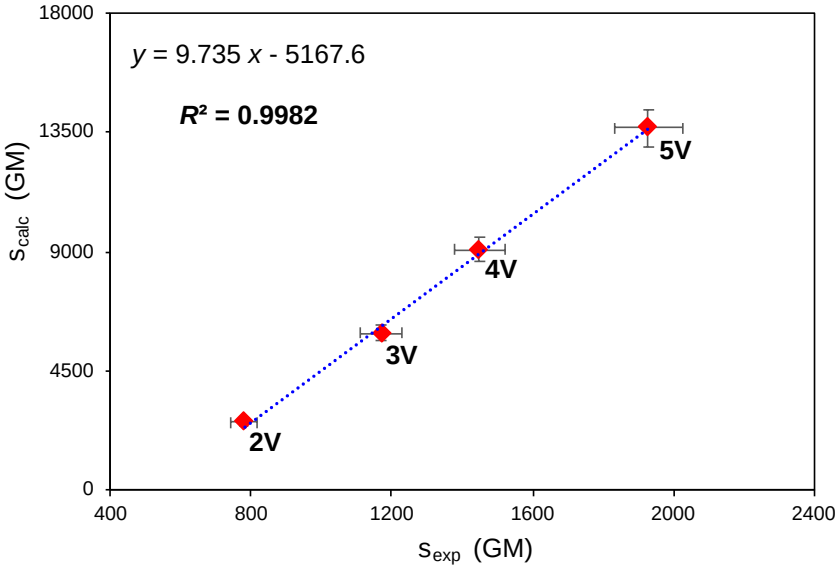

Fig. 2 Linear regression between experimental (in acetonitrile solvent) and theoretical 2PA cross-sections (in gas phase) of the **nV** (n=2-5) series of compounds.

It is worth noting that the dipolar counterparts of the **nV** and **nT** compounds, namely **2VD**, **4VD** (Table 1 and Figure S1, ESI) exhibit practically no 2PA, as well as the **2TD** and **4TD** species. This indicates that the quadrupolar NLO responses of the **nV** and **nT** compounds are not directly related to the dipolar one by an additive process. This is not surprising for mainly two reasons. Firstly, comparison of related dipoles and quadrupoles based on essential molecular orbital models reveals than one order of magnitude can often be stated between their respective two-photon cross-sections in favor of the quadrupoles.[16] Secondly, half-molecules such as **2VD** and **2TD** might not constitute proper dipolar equivalents of their respective quadrupolar parents **2V** and **2T** since the donor group (2-thienyl) has been halved compared to that present in **2V** or **2T** (5-(2,2'-bithiophene)). In this respect, **4VD** and **4TD** are certainly more representative dipolar equivalents of **2V** and **2T** and, accordingly with expectations, when the 2PA cross-sections of these molecules are compared, roughly one order of magnitude (or less) improvement in cross-section is observed when going from the dipole to the corresponding quadrupole.

Table 1 Experimental and SAOP/DZP calculated OPA (S1 state) and 2PA ω (eV) absorption energies and σ^{2PA} (GM) cross-sections of the **nV** and **nT** series of compounds.

Cmpd	Experimental[a]			Calculated		
	ω (eV)		σ^{2PA} (GM)	ω (eV)		σ^{2PA} (GM)
	OPA	2PA		OPA	2PA	
2V	2.73	1.63	780	2.17	1.20	2556
2VD				2.69	1.46	72
3V	2.63	1.61	1170	2.03	1.10	5938
4V	2.55	1.50	1450	1.88	1.00	9086
4VD				2.51	1.46	663
5V	2.54	1.61	1930	1.77	0.96	13637
2T				2.20	1.20	3857
2TD				2.77	1.45	78
3T				2.04	1.12	8845
4T				1.90	1.05	12255
4TD				2.58	1.40	369
5T				1.78	0.95	17912

[a] Ref. 4.

Comparing the **nV** and **nT** series of compounds, it appears that the NLO response of the latter is higher than the former. Moreover, a very good linear correlation (R^2 = 0.997) is found between the 2PA cross-sections of the two series of compounds (Figure S2, ESI). At

first sight, this result seemed surprising to us, since the HOMO-LUMO gaps (Table S1, ESI) for the **nT** compounds (except **2T**) are computed to be slightly higher than those of their **nV** counterparts. However, a closer look at the three-state (or essential state) model for the quadrupolar derivatives reveals that if such a simple approximation presently holds, the maximum 2PA cross-section value $(\sigma^{2PA})_{max}$ is given by eq. 1, where C is a constant term, μ_{ga} and $\mu_{ge,}$ the transition moments from the GS toward the OPA-forbidden state (***e***) and the OPA-allowed state (***a***), respectively, Γ_{ge} is a line-broadening factor for the former transition and E_{eg} and E_{ag} are the respective energies of these states from the GS.[16]

$$(\sigma^{2PA})_{max} = C.(\mu_{ga})^2(\mu_{ae})^2/[\Gamma_{ge}(2E_{ga}-E_{ge})]^2 \quad (1)$$

Thus, considering that the $C.(\mu_{ga})^2(\mu_{ae})^2/\Gamma_{eg}$ product is roughly constant for a series of homologous compounds, σ^{2PA} could be inversely proportional to $(2E_{ga}-E_{ge})^2$. Actually, this seems to be the case, since when E_{eg} is considered to be twice the energy determined for the 2PA transition by the SAOP calculation (Scheme 3) and E_{ag} to the energy for the OPA transition toward the allowed OPA state (Table 1), the $(2E_{ga}-E_{ge})^2$ term can be calculated for each quadrupolar compound. A very good linear correlation is found between these terms and the calculated $(\sigma^{2PA})_{max}$ values for the **nV** (R^2 = 0.98) and **nT** (R^2 = 0.93) series (see ESI). That being said, the $(2E_{ga}-E_{ge})^2$ term for corresponding **nV** and **nT** compounds is not always larger for **nV**. In other words, it does not originate from a more efficient detuning, since the $(2E_{ga}-E_{ge})^2$ terms are not systematically lower in the **nT** series. Actually, these terms are quite close for corresponding compounds of each series. Possibly, the difference in $(\sigma^{2PA})_{max}$ originates from the $(\mu_{ga})^2(\mu_{ae})^2$ product which must be larger in the **nT** series, explaining the larger cross-sections values found for **nT** derivatives and the correlation reported in Figure 2.

To attempt shedding some light on this hypothesis, frontier MOs (FMOs) of **nV** and **nT** were examined (Figures 3 and 4, and Table S1, ESI). Incidentally, it is worth noting here that the FMO diagrams computed using SAOP/DZP and PBE0/3-31G(d) are similar (see Figure S3, ESI for **2V** for instance) allowing the use of the latter MOs for our discussion, as well as the SAOP ones. As exemplified below for **2V** than for **2T**, it was stated that the HOMO energy is always higher for **nV** than for **nT** (-9.47 eV *vs.* -9.63 eV for n = 2), whereas the LUMO and LUMO+1 of **nT** are lower in energy than those of **nV** (-7.85 *vs.* -7.68 eV for the LUMOs for n = 2). These observations indicate that the electron-donating ability of the conjugated bridge is higher in the **nV** series, while its electron-accepting ability is higher in the **nT** series. This results in red-shifted transition energies from GS to the first allowed one-

photon state (***a*** in Scheme 3) for the **nV** derivatives. However, larger transition moments between the GS (***g***) and ***a*** excited states (μ_{ga}) are stated for the **nT** series making the $(\mu_{ga})^2(\mu_{ae})^2$ product larger for these compounds (if the second transition moment between the two first excited states (μ_{ae}) is considered as being roughly constant), in line with the increased 2PA cross-section stated for these compounds.

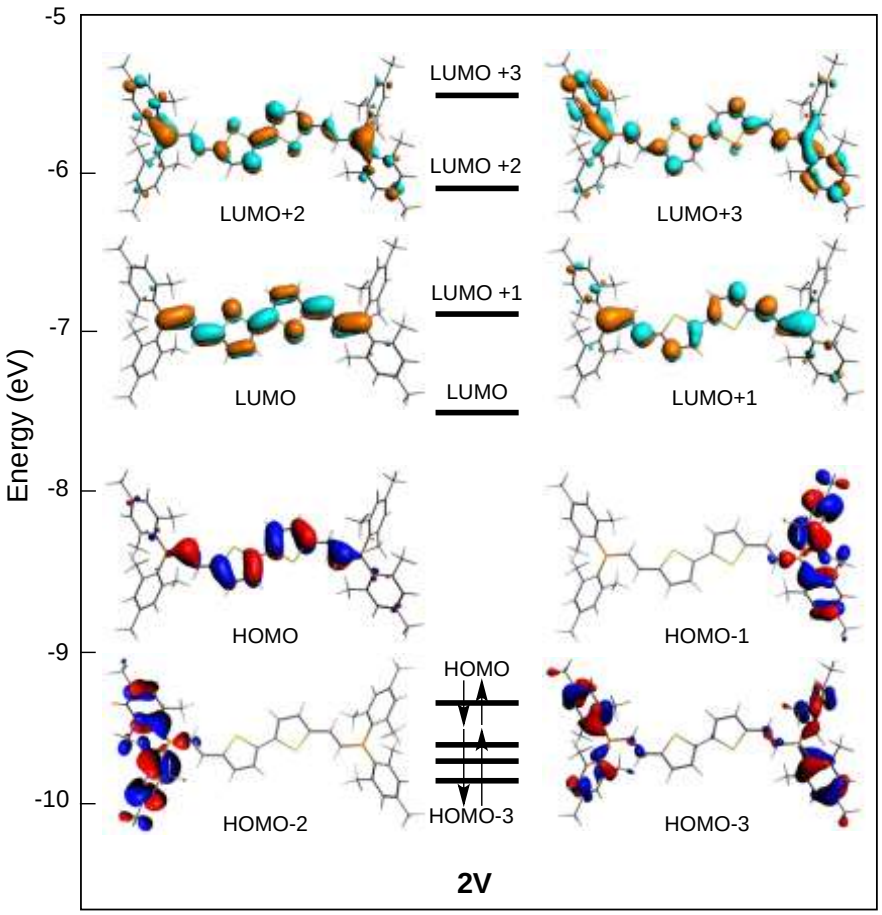

Fig. 3 Frontier MO diagram of **2V**. Contour values: ±0.03 au.

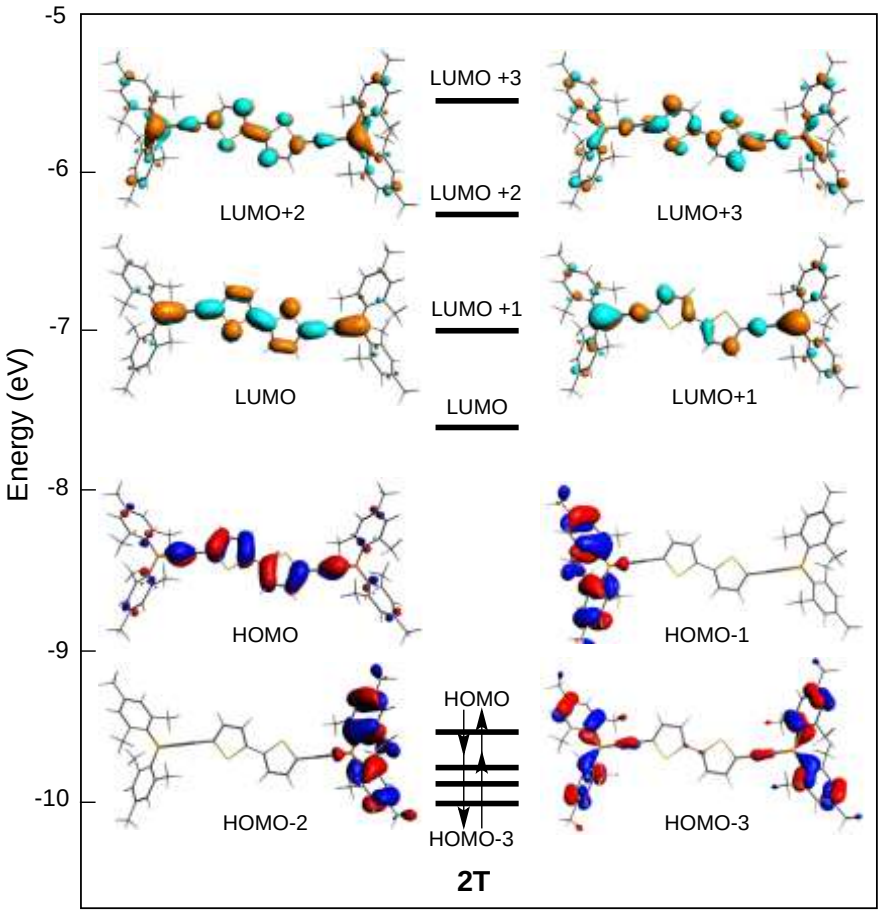

Fig. 4 Frontier MO diagram of **2T**. Contour values: ±0.03 au.

With these results in mind, let us consider now the **2TM-X** and **5M-X** series of compounds (Scheme 1). The main computed results are given in Table 2. In this table, the experimental data for **2TM-NMe$_3^+$** are also given for comparison. The simulated 2PA spectra of **2TM-X** (X = H, CN, NH_2) are displayed in Figure S4 (ESI). The frontier MO diagrams of all compounds are shown in Figures 5 (**2TM-NMe$_3^+$**) and 6 (**5M-NMe$_3^+$**) and Figure S5 (**2TM-X**; X = H, CN, NH_2). The excited state reached by the two-photon absorption is identified by its energy that must be twice the 2PA one. Identification of the one-photon forbidden states to which 2PA takes place reveals that the energy of these excited states with very weak oscillator strengths corresponds quite well to twice the computed 2PA energies (Table 2). For all compounds the low energy absorption corresponds to a HOMO to LUMO+1 transition, i.e., the S2 excited state, except for **2TM-NH$_2$** for which the excited state is S4.

Table 2 Experimental and SAOP/DZP calculated OPA and 2PA ω (eV) absorption energies and σ^{2PA} (GM) cross-sections of the **2TM-X** and **5M-X** series of compounds.

Cmpd	Experimental			Calculated		
	ω (eV)			ω (eV)		
	OPA	**2PA**	σ^{2PA} (GM)	**OPA** ω (f) transition[a]	**2PA**	σ^{2PA} (GM)
2TM-H				S1: 2.19 (0.690): H→L S2: 2.30 (0.002): H→L+1	1.15	2967
2TM-NH$_2$				S1: 2.26 (0.986): H →L S4: 2.40 (0.001): H → L+1	1.20	4919
2TM-CN				S1: 1.86 (0.500): H→L S2: 1.94 (0.001):H→L+1	0.98	4365
2TM-NMe$_3^+$	2.89	1.55 1.42	693 140	S1: 1.44 (0.563): H→L S2: 1.53 (0.0004): H→L+1 S20: 3.04 (0.003): H→LUMO+10	0.78 1.50	6269 134620
5M-H				S1: 1.86(1.298): H→L S2: 2.06(0.000): H→L+1	1.02	9423
5M-CN				S1: 1.55(0.817):H→L S2: 1.63(0.0001):H→L+1	0.82	9096
5M-NMe$_3^+$				S1: 1.05 (0.418): H→L S2: 1.12 (0.005): H→L+1 S6: 2.11 (0.000): H-1 →L	0.55 1.07	7482 112052

[a] Oscillator strength (f) and major transition (H = HOMO; L = LUMO).

The MO diagrams of the **2TM-X** series of compounds shown in Figure 5 (X = NMe_3^+) and Figure S6 (X = H, CN, NH_2, ESI) indicate that the LUMO and LUMO+1 energies are lower when more electron-attracting groups are attached to the phenyl rings tethered to the terminal $BMes_2$ groups, reminding that the latter MO is strongly involved in the one-photon forbidden/two-photon-allowed electronic transition toward the S2 state. In more detail, we can

state that in line with eq. 1, there is a good linear correlation with the $(2E_{ga}\text{-}E_{ge})^{-2}$ term (R^2 = 0.97) for all compounds except for **2TM-NH$_2$**. When the data of the latter is incorporated, the correlation coefficient drops (R^2 = 0.63), in line with the fact that eq. 1 is certainly no more valid for this compound. This reveals that more than three states are needed to describe the 2PA behavior of this compound, in line with the occurrence of several low-lying excited states close in energy. Thus, it appears that for all **2TM-X** derivatives, except **2TM-NH$_2$**, the electron transfer from the central electron-donating bridge to the substituted $BMes_2$ moieties (excitation to the S_2 or S_4 states) is determining for the 2PA and, without any surprise, it is larger with the strongest electron-withdrawing group. From Table 2, it can be seen that the computed cross-sections follow the order **2TM-H** < **2TM-CN** < **2TM-NMe$_3^+$** consistent with the $(2E_{ga}\text{-}E_{ge})^{-2}$ ordering, which also roughly follows the reverse HOMO-LUMO gap trend. The differences of the electron densities between the state S_2 and the ground state S_0 (Figure S6, ESI) show a variation of the dipole moment that follows the same ordering, suggesting also some positive influence on the 2PA magnitude *via* the HOMO-LUMO transition moments (*e.g.*, μ_{ga} in eq. 1). We note also a slight variation of the oscillator strength along this series of compounds reflecting similar changes in the transition moment μ_{ga}. In line with the observed correlation cited above, such a change is certainly balanced by a reverse change in μ_{ae} for each of these compounds, except **2TM-NH$_2$**, leading to a nearly constant numerator in eq. 1. Thus, the increased CT character leading to a lower HOMO-LUMO gap for **2TM-NMe$_3^+$** can nicely explain the significantly better 2PA response observed for this compound. In contrast, for **2TM-NH$_2$**, the presence of the strongly electron-releasing amino substituents which significantly perturb the FMO ordering, results in a more complex situation and additional excited states become determining for the 2PA response, explaining the deviation of the 2PA cross-section of that compound from correlations based on a three-state model. This compound exhibits nevertheless also a high 2PA cross-section that might now be correlated with the high electron-donating ability of the conjugated bridge and the change in the nature of the first two-photon-allowed excited state of this compound.

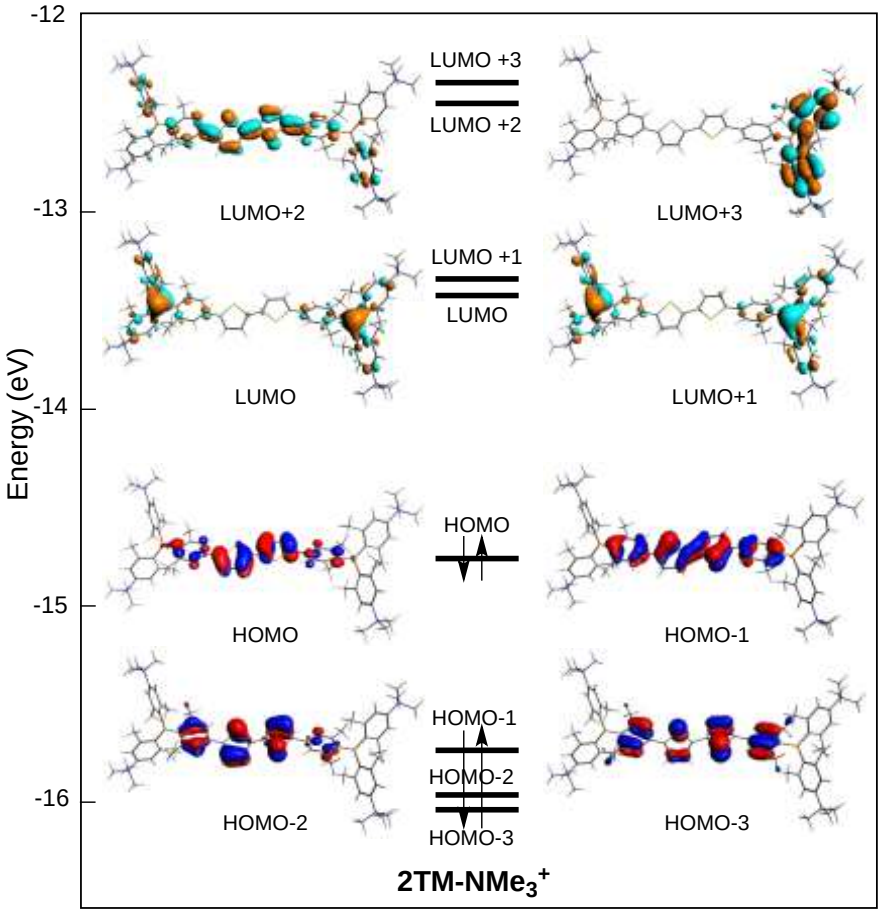

Fig. 5 Frontier MO diagram of **2TM-NMe$_3^+$**. Contour values: ±0.03 au.

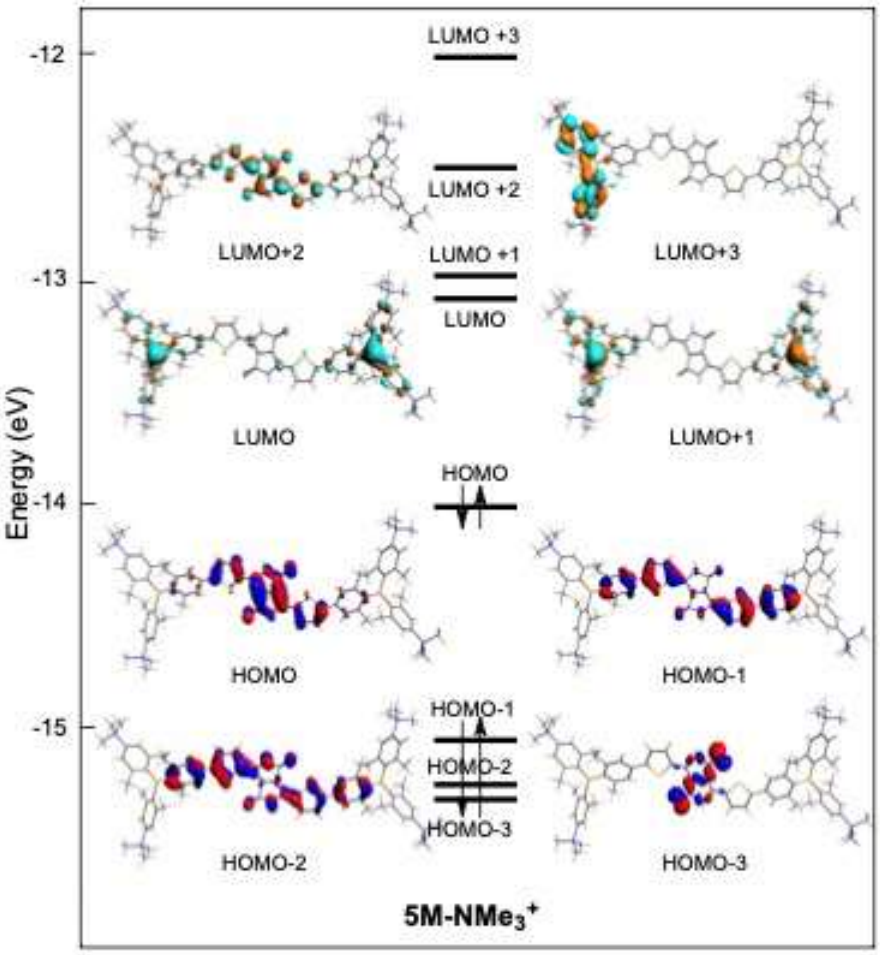

Fig. 6 Frontier MO diagrams of **5M-NMe$_3^+$**. Contour values: ±0.03 au.

For **5M-X** compounds (X = H, CN, NMe_3^+), opposite statements can be made compared to their **2TM-X** analogues. Though a very similar ordering is found for their first FMOs and excited states, and a good linear correlation between the 2PA of these compounds and the $(2E_{ga}\text{-}E_{ge})^{-2}$ term can be evidenced (R^2 = 0.99), this time, the slope of this correlation is opposite to expectations and the computed cross-sections follow the order **5M-H** > **5M-CN** > **5M-NMe_3^+** which is roughly opposite to the decrease of the HOMO-LUMO gap for these compounds, questioning the adequacy of a three-state model (eq. 1) to describe their 2PA properties. Obviously, the much larger changes in the transition moment to the first OPA-allowed state (μ_{ga}) dominate the evolution of 2PA, contrary to what was observed for **2TM-X** (X = H, CN, NMe_3^+) series.

Comparatively to **4V** (Table 1), **2TM-H**, that contains the same number of aromatic rings in the conjugated bridge, differs by the values of the 2PA cross-sections as well as by the 2PA energy. Indeed, the σ^{2PA} value is equal to 9086 GM for **4V** but only to 2967 for **2TM-H**. In the latter compound phenyl rings have replaced the alkyne units (see Schemes 1 and 2). Thus, the latter exhibits a longer conjugated bridge. This result is consistent with the smaller HOMO-LUMO gap of **4V** with respect to that of **2TM-H** (1.57 *vs.* 2.03 eV, respectively; SAOP/DZP calculation, Table S1, ESI) and with the better planarity of the π-manifold in the former. This result is also consistent with the better electron-attracting ability within the **4V** species that is reflected by its lower LUMO energy comparatively to the **2TM-H** ones.

Finally, two peaks appear in the simulated 2PA spectra of **2TM-NMe_3^+** and **5M-NMe_3^+** (Figure 7, left). In particular, it is worth noting that the 2PA peaks at higher energies have much larger cross-sections than the peaks at lower energies. The high-energy peaks correspond to transitions to higher excited states, *i.e.*, S20 for **2TM-NMe_3^+** and S6 for **5M-NMe_3^+** and, by definition, they cannot be modeled by a three-state model (eq. 1). The corresponding transitions are given in Table 2 and the involved MO is depicted in Figure S7 (ESI). Note that these excitations might have quite close transition moments since the peak found for **5M-NMe_3^+** is slightly broader than that computed for **2TM-NMe_3^+** (Figure 7). As it can be seen upon comparison of the peaks at lower energy, the maximum cross-section is higher for **2TM-NMe_3^+** while the reverse is observed for the peak at higher energy.

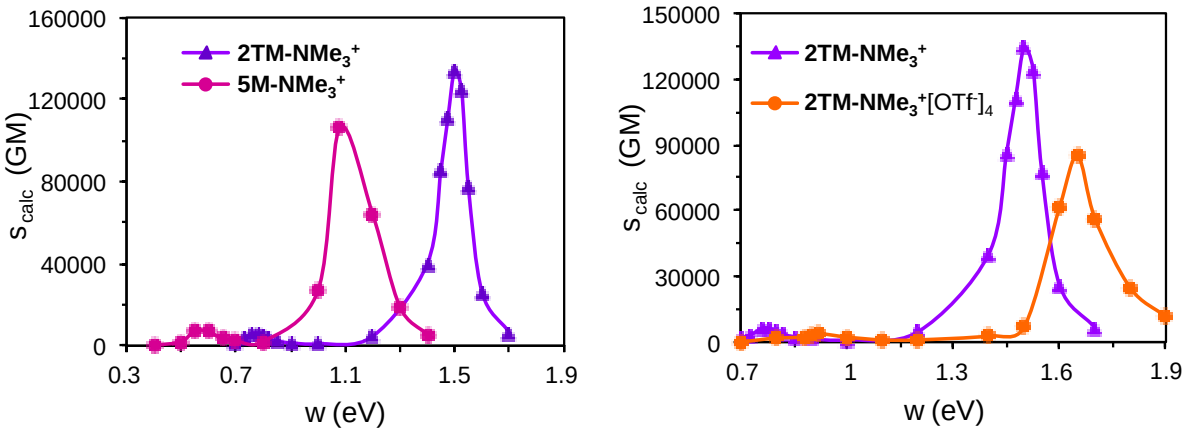

Fig. 7 Comparison of the simulated 2PA spectra of **2TM-NMe$_3^+$** and **5M-NMe$_3^+$** (left) and **2TM-NMe$_3^+$** and **2TM-NMe$_3^+$**[OTf$^-$]$_4$ (right).

The ionic systems exhibit 2PA cross-sections higher than the neutral ones. Solvation effects should be more important for such cationic species. The counterions, four triflate anions here for **2TM-NMe$_3^+$**, certainly play a role, especially in the solid state where they are supposed to be located closer to the NMe$_3^+$ groups of the tetra-cationic molecule than in solution. The structures of the optimized geometries of the isolated cationic **2TM-NMe$_3^+$** and of the neutral **2TM-NMe$_3$**[OTf]$_4$ molecules are given in Figure S8 (ESI). When considering the surrounding triflate (OTf$^-$) counter-ion, its main effect is a drastic reduction of the maximum 2PA cross-section, as can be seen in Figure 7 (right). This is probably due to their negative charge, which likely reduces the attracting ability of the substituted BMes$_2$ moieties.

Normalizing the NLO response of a given molecule by the effective number of π electrons (N_{eff}) constitutes a simple and practical way to correct its NLO response for the size of its π manifold.[18,19] When this is done for our computed 2PA cross-sections (Table 2), the most efficient systems according to the resulting figures (Table S3, ESI) are **2T** followed by **5M-H**. Based on these figures of merit it appears that, contrarily to a common belief, the ethynyl-bridged mesityl boranes derivatives **2T** should be better two-photon absorbers that their ethenyl bridged homologues **2V**, which is not so surprising given the constancy of N_{eff} between **nT** and **nV** analogues. Then, the performance of the new **5M-X** systems as two-photon absorbers over the known **2TM-X** is clearly pointed out. Overall, these results confirm also further the interest of using the new water-soluble **2TM-NMe$_3^+$** and **5M-NMe$_3^+$** quadrupoles for bioimaging studies.

Conclusion

2PA properties of a series of quadrupolar dimesitylboryl ($BMes_2$) derivatives containing different conjugated thiophene oligomers spanning terminal $BMes_2$ moieties have been investigated theoretically. Interestingly, SAOP/DZP DFT calculations gave correct trends regarding the cross-section variation with the length of the thiophene oligomer in the **2V**-**5V** series of compounds. Results confirmed that the excited state reached by the two-photon absorption is the S2 state corresponding to the HOMO→LUMO+1 transition for all compounds that were studied. The 2PA of these compounds seems to be mainly dependent on the energy gap between the GS and the two first excited states. Its evolution can be qualitatively modeled by a three-state model, explaining the huge impact of the underestimation of the actual energy gaps of these molecules by the SAOP method on the magnitude of the calculated cross-sections, while remaining qualitatively correct.

Results have also indicated that replacing the terminal ethynyl double bonds in the **nV** species by alkynyl triple bonds in the **2T**-**5T** compounds leads to an increase of the 2PA cross-sections. The tetracationic compounds **2TM-NMe$_3^+$** and **5M-NMe$_3^+$** that contain one NMe_3^+ groups attached to the phenyl rings of the $BMes_2$ moieties were shown experimentally to present very high 2PA cross-sections. This is confirmed by our computations that also show two 2PA peaks at different wavelengths, the low energy one corresponding to the absorption to the S2 excited state, whereas the second one to higher excited states. Neutral **2TM-X** and **5M-X** systems, where CN groups replace NMe_3^+ groups, should exhibit lower 2PA cross-sections than the ionic **2TM-NMe$_3^+$** and **5M-NMe$_3^+$** counterparts. For these compounds, the adequacy of the three-state model to qualitatively predict the 2PA properties is more questionable, especially for the **5M-X** series (X = H, CN, NMe_3^+). Due to their lower solubility in polar solvents, these compounds should be far less interesting for two-photon bio-imaging purposes.

Conflicts of interest

There are no conflicts to declare.

Acknowledgements

The financial support of ANR (Isogate Project) is acknowledged as well as GENCI-IDRIS and GENCI-CINES for computing time allocation (Grant 2019-2020-080649).

References

1- C. D. Entwistle and T. B. Marder, *Chem. Mater.* **2004**,16, 4574–4585.

2- Z. Yuan, C. D. Entwistle, J. C. Collings, D. Albesa-Jové, A. S. Batsanov, J. A. K. Howard, N. J. Taylor, H. Martin Kaiser, D. E. Kaufmann, S.-Y. Poon, W.-Y. Wong, C. Jardin, S. Fathallah, A. Boucekkine, J.-F. Halet and Todd B. Marder, *Chem. Eur. J.* **2006**, *12*, 2758–2771.

3- C. D. Entwistle, J. C. Collings, A. Steffen, L.-O. Palsson, A. Beeby, D. Albesa-Jové , J. M. Burke, A. S. Batsanov, J. A. K. Howard, J. A. Mosely, S.-Y. Poon, W.-Y. Wong, F. Ibersiene, S. Fathallah, A. Boucekkine, J.-F. Halet and T. B. Marder. *J. Mater. Chem.* **2009**, *19*, 7532–7544.

4- L. Ji, R. M. Edkins, L. J. Sewell, A. Beeby, A. S. Batsanov, K. Fucke, M. Drafz, J. A. K. Howard, O. Moutounet, F. Ibersiene, A. Boucekkine, E. Furet, Z. Q. Liu, J.-F. Halet, C. Katan and Todd B. Marder, *Chem. Eur. J.* **2014**, *20*, 13618–13635.

5- S. Griesbeck, Z. Zhang, M. Gutmann,T. Lehmann, R. M. Edkins, G. Clermont, A. N. Lazar, M. Haehnel, K. Edkins, A. Eichhorn, M. Blanchard-Desce, L.Meinel and T. B. Marder, *Chem. Eur. J.* **2016**, *22*, 14701–14706.

6- S. Griesbeck, E. Michail, C. G. Wang, H. Ogasawara, S. Lorenzen, L. Gerstner, T. Zang, J. Nitsch, Y. Sato, R. Bertermann, M. Taki, C. Lambert, S. Yamaguchi and T. B. Marder, *Chem. Sci*.. **2019**, *10*, 5405–5422.

7- G.S. He, L.S. Tan, Q. Zheng and P.N. Prasad, *Chem. Rev.* **2008**, *108*, 1245–1330.

8- K. D. Belfield, X. Ren, E. W. Van Stryland, D. J. Hagan, V. Dubikovski and E. J. Meisak, *J. Am. Chem. Soc*. **2000**, *122*, 1217–1219.

9- D. Dini, M. J. F. Calvete and M. Hanack, *Chem. Rev.* **2016**, *116*, 13043–13233.

10- M. Pawlicki, H. A. Collins, R. G. Denning and H. L. Anderson, *Angew. Chem. Int. Ed*., **2009**, *48*, 3244–3266.

11- H. Zhongwei, J. Autschbach and L. Jensen. *J. Chem.Theory Comput.* **2016**, *12*, 1294–1304.

12- *ADF* Amsterdam Density Functional; Scientific Computing & Modelling: Amsterdam. The Netherlands, 2019. http://www.scm.com.

13- P. R. T. Schipper, O. V. Gritsenko, S. J. A. van Gisbergen and E. J. Baerends. *J. Chem. Phys.* **2000**, *112*, 1344–1352.

14- C. Adamo and V. Barone, *J. Chem. Phys.* **1999**, *110*, 6158−6169.

15- Frisch. M. J. et al. *Gaussian 16, Revision A.03* Edition. Gaussian. Inc. Wallingford CT

16- M. Bazourkas and M. Blanchard-Desce, *J. Chem. Phys.* **2000**, *113*, 3951–3959.

17- A. Amar, A. Boucekkine, F. Paul and O. Mongin, *Theoret. Chem. Acc.* **2019**, *138*, 105.

18- M. G. Kuzyk, *J. Chem. Phys.* **2003**, *119*, 8327–8334.

19- M. G. Kuzyk, *J. Mater. Chem.* **2009**, *19*, 7444–7465.